

A new spectral apparent horizon finder for 3D numerical relativity

Lap-Ming Lin^{1,2,3‡} and Jérôme Novak^{3§}

¹ Department of Physics and Institute of Theoretical Physics, The Chinese University of Hong Kong, Hong Kong, China

² Department of Physics, University of Hong Kong, Hong Kong, China

³ Laboratoire de l'Univers et de ses Théories, UMR 8102 du CNRS, Observatoire de Paris, F-92195 Meudon Cedex, France

Abstract. We present a new spectral-method-based algorithm for finding apparent horizons in three-dimensional space-like hypersurfaces without symmetries. While there are already a wide variety of algorithms for finding apparent horizons, our new algorithm does not suffer from the same weakness as previous spectral apparent horizon finders: namely the monopolar coefficient ($\ell = 0$ in terms of the spherical harmonics decomposition) needed to be determined by a root-finding procedure. Hence, this leads to a much faster and more robust spectral apparent horizon finder. The finder is tested with the Kerr-Schild and Brill-Lindquist data. Our finder is accurate and is as efficient as the currently fastest methods developed recently by Schnetter (2003 *Class. Quantum Grav.* **20**, 4719) and Thornburg (2004 *Class. Quantum Grav.* **21**, 743). At typical resolutions it takes only 0.5 second to find the apparent horizon of a Kerr-Schild black hole with $a = 0.9M$ to the accuracy $\sim 10^{-5}$ for the fractional error in the horizon's location on a 2 GHz processor.

PACS numbers: 04.25.Dm, 04.70.Bw, 02.70.Hm

1. Introduction

Apparent horizons play an important role in numerical relativity for spacetimes containing black hole(s). Being defined locally in time (see section 2), the apparent horizon(s) can readily be computed from the data on each hypersurface during a numerical evolution in $(3 + 1)$ numerical relativity. In contrast, the event horizon is a global property and can be determined approximately only when the spacetime has essentially settled down to a stationary state. Once the spacetime has settled down, the event horizon can be found at all previous times by integrating null geodesics backwards in time (e.g., [1, 2, 3, 4]). As it (if exists) must be inside an event horizon [5], the apparent horizon is an important tool to track the location and movement of black hole(s) in a numerically generated spacetime. Furthermore, the surface of an apparent horizon also provides a natural boundary within which the spacetime region can be excised from the computational domain in order to handle the physical singularities inside a black hole [6, 7, 8] (also see, e.g., [9, 10, 11, 12] for black hole simulations without excision). In the new concept of a ‘dynamical horizon’ (see

‡ Email address: lmlin@phy.cuhk.edu.hk

§ Email address: Jerome.Novak@obspm.fr

[13, 14] for reviews), apparent horizons are essentially the cross sections of the (three-dimensional space-like) dynamical horizon on the hypersurfaces. It has recently been shown in this context that the areas of the apparent horizons satisfy a causal evolution equation and give a positive bulk viscosity in a viscous fluid analogy [15]. This is in contrast to the event horizon which yields a noncausal evolution and a negative bulk viscosity.

A wide variety of algorithms for finding apparent horizons have been proposed in the past decade. We refer the reader to the review article by Thornburg [16] (and references therein) for details. In this paper, we present a new apparent horizon finder which is based on spectral methods. While the spectral-method-based algorithm for finding apparent horizons was first proposed by Nakamura *et al* [17] more than 20 years ago, our new approach does not suffer from the same weakness as in the Nakamura *et al* algorithm: namely the $\ell = 0$ coefficient of the spherical harmonics decomposition of the apparent horizon's surface needed to be determined by a root-finding procedure. Hence, our algorithm leads to a more robust and efficient spectral apparent horizon finder. We have tested our finder with analytic solutions for single and two black-hole spacetimes. Our finder is as efficient as the currently fastest algorithms developed by Schnetter [18] and Thornburg [19].

This paper is organized as follows. In section 2 we present the notations and various definitions. In section 3 we briefly review the Nakamura *et al.* algorithm; we describe our spectral algorithm and the numerical procedure in section 4. Section 5 presents tests with analytic solutions to assess the accuracy, robustness, and efficiency of our finder. Finally, we summarize our results in section 6. Latin (Greek) indices go from 1 to 3 (0 to 3).

2. Notations and definitions

Given a space-like hypersurface Σ with future-pointing unit normal n^μ , the 3-metric $\gamma_{\mu\nu}$ induced by the spacetime metric $g_{\mu\nu}$ onto Σ is

$$\gamma_{\mu\nu} := g_{\mu\nu} + n_\mu n_\nu. \quad (1)$$

Let S be a closed smooth (two-dimensional) surface embedded in Σ , and let s^μ be the outward-pointing unit normal of S , which is spacelike and also normal to n^μ (i.e., $s_\mu s^\mu = 1$ and $s_\mu n^\mu = 0$). The 3-metric $\gamma_{\mu\nu}$ now induces a 2-metric on S :

$$m_{\mu\nu} := \gamma_{\mu\nu} - s_\mu s_\nu. \quad (2)$$

Let k^μ be the tangents of the outgoing future-pointing null geodesic whose projection on Σ is orthogonal to S . We have (up to an overall factor)

$$k^\mu = s^\mu + n^\mu, \quad (3)$$

on the 2-surface S .

The expansion of the outgoing null geodesics is

$$\Theta = \nabla_\mu k^\mu, \quad (4)$$

where ∇_μ is the covariant derivative associated with $g_{\mu\nu}$. In terms of three-dimensional quantities, on the 2-surface S , the expansion can be written as (see, e.g., [20])

$$\Theta = D_i s^i - K + s^i s^j K_{ij}, \quad (5)$$

where D_i is the covariant derivative associated with γ_{ij} , K_{ij} is the extrinsic curvature of Σ and K is the trace of K_{ij} . The expansion can also be written as

$$\Theta = m^{ij} (D_i s_j - K_{ij}). \quad (6)$$

The 2-surface S is called a marginally trapped surface if $\Theta = 0$ everywhere on S . We shall call here the outermost of such surfaces (which is a marginally outer trapped surface - MOTS) the apparent horizon.

To parameterize the apparent horizon, we assume that the topology of S is a 2-sphere, and S is star-shaped around the coordinate origin $r = 0$, which means that for every point M inside S , the straight line connecting the origin to M is entirely inside S [21]. The position of the apparent horizon can then be represented as

$$F(r, \theta, \varphi) := r - h(\theta, \varphi) = 0, \quad (7)$$

where (r, θ, φ) are the standard spherical coordinates. The function h measures the coordinate distance to the horizon's surface in the direction (θ, φ) . With this parametrization, the unit normal s^i is given by

$$s^i = \frac{D^i F}{(\gamma^{ij} D_i F D_j F)^{1/2}} := \frac{D^i F}{|DF|}, \quad (8)$$

where $D^i := \gamma^{ij} D_j$. The expansion (equation (6)) becomes

$$\Theta = m^{ij} \left(\frac{D_i D_j F}{|DF|} - K_{ij} \right), \quad (9)$$

where the condition $m^{ij} s_j = 0$ has been used.

3. The Nakamura *et al* algorithm

In this section, we give a brief review of the algorithm adopted by Nakamura *et al* [17] for finding apparent horizon based on spectral methods. They expand h in spherical harmonics:

$$h(\theta, \varphi) = \sum_{\ell=0}^{\ell_{\max}} \sum_{m=-\ell}^{\ell} a_{\ell m} Y_{\ell}^m(\theta, \varphi). \quad (10)$$

They rewrite the apparent horizon equation $\Theta = 0$ as||

$$\Delta_{\theta\varphi} h = \rho \Theta + \Delta_{\theta\varphi} h, \quad (11)$$

where $\Delta_{\theta\varphi}$ is the flat Laplacian operator on a 2-sphere defined by

$$\Delta_{\theta\varphi} h := h_{,\theta\theta} + \cot \theta h_{,\theta} + \sin^{-2} \theta h_{,\varphi\varphi}. \quad (12)$$

The positive scalar function ρ is chosen such that the term $h_{,\theta\theta}$ cancels on the right-hand side (RHS). Using the fact that the Y_{ℓ}^m are an orthogonal set of eigenfunctions of $\Delta_{\theta\varphi}$,

$$\Delta_{\theta\varphi} Y_{\ell}^m = -\ell(\ell+1) Y_{\ell}^m, \quad (13)$$

we obtain the relation (with $d\Omega = \sin \theta d\theta d\varphi$)

$$-\ell(\ell+1) a_{\ell m} = \int_S Y_{\ell}^{m*} (\rho \Theta + \Delta_{\theta\varphi} h) d\Omega. \quad (14)$$

This equation can be used to solve for the coefficients $a_{\ell m}$ via an iteration procedure. However, the value of a_{00} has to be determined at each iteration step by solving for the root of

$$\int_S Y_0^{0*} (\rho \Theta + \Delta_{\theta\varphi} h) d\Omega = 0. \quad (15)$$

|| We follow the notation of Gundlach [22].

The main disadvantage of the above scheme is that the coefficient a_{00} has to be determined separately by equation (15). As pointed out by Gundlach [22], solving equation (15) by any iteration method is as computationally expensive as many steps of the main iteration loop. Furthermore, equation (15) may have multiple roots or none. In those cases, each root or each minimum (if there is no root) should be investigated separately [23]. This clearly reduces the efficiency of the algorithm significantly.

4. Our algorithm

4.1. Master equation for apparent horizon

Our spectral-method-based algorithm uses a similar ansatz (11) as Nakamura *et al* [17]. The main difference is that we do not need to determine a_{00} separately. Hence, this leads to a more robust and efficient apparent horizon finder based solely on the spectral method[¶].

To begin, we first introduce a flat metric f_{ij} on the hypersurface Σ . The components of the flat metric with respect to the spherical coordinates (r, θ, φ) , and the associated natural basis $(\frac{\partial}{\partial r}, \frac{\partial}{\partial \theta}, \frac{\partial}{\partial \varphi})$, are $f_{ij} = \text{diag}(1, r^2, r^2 \sin^2 \theta)$. Let \bar{D}_i be the covariant derivative associated with f_{ij} . The expansion function Θ (equation (9)) can now be written as

$$\Theta = (\gamma^{ij} - s^i s^j) [|DF|^{-1} (\bar{D}_i \bar{D}_j F - \Delta_{ij}^m \bar{D}_m F) - K_{ij}], \quad (16)$$

where the tensor field Δ_{ij}^m is defined by

$$\Delta_{ij}^m := \frac{1}{2} \gamma^{mn} (\bar{D}_i \gamma_{jn} + \bar{D}_j \gamma_{in} - \bar{D}_n \gamma_{ij}). \quad (17)$$

We have also used the following relation between the two covariant derivatives D_i and \bar{D}_i :

$$D_i V_j = \bar{D}_i V_j - \Delta_{ij}^m V_m, \quad (18)$$

where V^j is an arbitrary 3-vector on Σ_t .

Motivated by the recently proposed fully constrained-evolution scheme for numerical relativity [24], we define a conformal factor Ψ by

$$\Psi := \left(\frac{\det \gamma_{ij}}{\det f_{ij}} \right)^{1/12}, \quad (19)$$

and also a tensor field h^{ij} by

$$\gamma^{ij} = \Psi^{-4} (f^{ij} + h^{ij}). \quad (20)$$

We also expand all tensor fields onto the following spherical basis:

$$\mathbf{e}_{\hat{r}} := \frac{\partial}{\partial r}, \quad \mathbf{e}_{\hat{\theta}} := \frac{1}{r} \frac{\partial}{\partial \theta}, \quad \mathbf{e}_{\hat{\varphi}} := \frac{1}{r \sin \theta} \frac{\partial}{\partial \varphi}. \quad (21)$$

This basis is orthonormal with respect to the flat metric: $f_{\hat{i}\hat{j}} = \text{diag}(1, 1, 1)$. Here and afterwards, we denote the tensor indices associated with this basis with a hat. The expansion function now becomes

$$\Theta = \Psi^{-4} |DF|^{-1} f^{\hat{i}\hat{j}} \bar{D}_{\hat{i}} \bar{D}_{\hat{j}} F + \left(\Psi^{-4} h^{\hat{i}\hat{j}} - s^{\hat{i}} s^{\hat{j}} \right) |DF|^{-1} \bar{D}_{\hat{i}} \bar{D}_{\hat{j}} F$$

[¶] See [22] for Gundlach's "fast flow" algorithm which combines the spectral algorithm of Nakamura *et al* and the so-called curvature flow method (see also [16] for discussion).

$$- \left(\gamma^{\hat{i}\hat{j}} - s^{\hat{i}} s^{\hat{j}} \right) \left(|DF|^{-1} \Delta^{\hat{m}}_{\hat{i}\hat{j}} \overline{D}_{\hat{m}} F + K_{\hat{i}\hat{j}} \right). \quad (22)$$

Now let us consider the first term on the RHS of this equation:

$$\begin{aligned} \Psi^{-4} |DF|^{-1} f^{\hat{i}\hat{j}} \overline{D}_{\hat{i}} \overline{D}_{\hat{j}} F &= \Psi^{-4} |DF|^{-1} \left(\overline{D}_{\hat{r}} \overline{D}_{\hat{r}} F + \overline{D}_{\hat{\theta}} \overline{D}_{\hat{\theta}} F + \overline{D}_{\hat{\varphi}} \overline{D}_{\hat{\varphi}} F \right) \\ &= \frac{-1}{\Psi^4 |DF| r^2} \left(h_{,\theta\theta} + \cot \theta h_{,\theta} + \sin^{-2} \theta h_{,\varphi\varphi} - 2r \right) \\ &= \frac{-1}{\Psi^4 |DF| h^2} \left(\Delta_{\theta\varphi} h - 2h \right), \end{aligned} \quad (23)$$

where we have set $r = h(\theta, \varphi)$ for the apparent horizon in the last equality. In equation (23), we have used the following relation for the components of the covariant derivative $\overline{D}_{\hat{j}}$ of a 3-vector $V^{\hat{i}}$ in the orthonormal basis $\{\mathbf{e}_{\hat{i}}\}$:

$$\overline{D}_{\hat{j}} V_{\hat{i}} = e_j^k \frac{\partial}{\partial x^k} V_{\hat{i}} - \hat{\Gamma}_{\hat{i}\hat{j}}^{\hat{k}} V_{\hat{k}}, \quad (24)$$

where $e_j^k := \text{diag}[1, 1/r, 1/(r \sin \theta)]$. The $\hat{\Gamma}_{\hat{i}\hat{j}}^{\hat{k}}$ are the connection coefficients of $\overline{D}_{\hat{k}}$ associated with $\{\mathbf{e}_{\hat{i}}\}$. The non-vanishing components are

$$\hat{\Gamma}_{\hat{\theta}\hat{\theta}}^{\hat{r}} = -\hat{\Gamma}_{\hat{r}\hat{\theta}}^{\hat{\theta}} = -\frac{1}{r}, \quad \hat{\Gamma}_{\hat{\varphi}\hat{\varphi}}^{\hat{r}} = -\hat{\Gamma}_{\hat{r}\hat{\varphi}}^{\hat{\varphi}} = -\frac{1}{r}, \quad \hat{\Gamma}_{\hat{\varphi}\hat{\varphi}}^{\hat{\theta}} = -\hat{\Gamma}_{\hat{\theta}\hat{\varphi}}^{\hat{\varphi}} = \frac{-1}{r \tan \theta}. \quad (25)$$

Equations (22) and (23) suggest that, instead of the ansatz (11) as taken by Nakamura *et al*, it is more appropriate to rewrite the apparent horizon equation $\Theta = 0$ as

$$\Delta_{\theta\varphi} h - 2h = \lambda \Theta + \Delta_{\theta\varphi} h - 2h, \quad (26)$$

where the scalar function λ is chosen to be $\lambda = \Psi^4 |DF| h^2$ such that the combination $\Delta_{\theta\varphi} h - 2h$ cancels on the RHS of this equation. Hence, the master equation that we solve in our algorithm is

$$\begin{aligned} \Delta_{\theta\varphi} h - 2h &= \Psi^4 |DF| h^2 \left[\left(\Psi^{-4} h^{\hat{i}\hat{j}} - s^{\hat{i}} s^{\hat{j}} \right) |DF|^{-1} \overline{D}_{\hat{i}} \overline{D}_{\hat{j}} F \right. \\ &\quad \left. - \left(\gamma^{\hat{i}\hat{j}} - s^{\hat{i}} s^{\hat{j}} \right) \left(|DF|^{-1} \Delta^{\hat{m}}_{\hat{i}\hat{j}} \overline{D}_{\hat{m}} F + K_{\hat{i}\hat{j}} \right) \right]. \end{aligned} \quad (27)$$

The expansion coefficients are now determined by solving the following equation iteratively:

$$a_{\ell m} = \frac{-1}{\ell(\ell+1)+2} \int_S Y_{\ell}^{m*} (\lambda \Theta + \Delta_{\theta\varphi} h - 2h) d\Omega. \quad (28)$$

This equation applies for all $\ell \geq 0$, and hence a_{00} is not treated specially. In [25], Shibata developed an apparent horizon finder based essentially on the same form of equation (26). However, he solved the equation using the finite-differencing method without pointing out the key advantage that, if solved by the spectral method, the coefficient a_{00} (as determined by our equation (28) and his equation (1.3) in [25]) does not need to be solved by the root-finding procedure. In this work, we solve the algorithm for the first time with spectral method. The difference between equations (28) and (14) leads to a dramatic improvement in the efficiency and robustness of spectral-method-based algorithms for finding apparent horizons.

4.2. Numerical procedure

For given 3-metric γ_{ij} and extrinsic curvature K_{ij} on a hypersurface Σ , equation (27) represents a nonlinear elliptic equation for the function h . We solve this equation iteratively by considering the RHS of the equation as a source term for the linear operator $\Delta_{\theta\varphi} - 2$ acting on h . We use a multidomain spectral method to solve the elliptic equation [21, 26]. The code is constructed upon the C++ library LORENE [27], and is publicly available.

The numerical iteration procedure is briefly described here. Assume that the data $(\gamma_{\hat{i}\hat{j}}, K_{\hat{i}\hat{j}})$ are given on Σ . The conformal factor Ψ and the tensor field $h^{\hat{i}\hat{j}}$ are then calculated by equations (19) and (20), respectively. Assume that an initial guess for the function $h(\theta, \varphi)$ is chosen (equivalently for the spectral coefficients $a_{\ell m}$). The iteration processes are as follows.

- (i) At the n th iteration step, the function $h^{(n)}$ is determined by the coefficients $a_{\ell m}^{(n)}$ (with the superscript (n) labels the iteration steps). The level-set function F and the unit normal vector s^i are then obtained from $h^{(n)}$ (see section 2).
- (ii) The spectral coefficients at the next iteration step are calculated by equation (28):

$$a_{\ell m}^{(n+1)} = \frac{-1}{\ell(\ell+1)+2} \int_S Y_\ell^{m*} S^{(n)} d\Omega, \quad (29)$$

where $S^{(n)}$ represents the RHS of equation (27) evaluated from $a_{\ell m}^{(n)}$. The new function $h^{(n+1)}$ is then obtained from $a_{\ell m}^{(n+1)}$ by equation (10).

- (iii) The difference between $h^{(n+1)}$ and $h^{(n)}$ is calculated. The iteration procedure continues until the maximum value of the difference throughout the whole angular grid (θ_i, φ_j) is smaller than some prescribed value ϵ_h .

5. Tests

5.1. Kerr-Schild data

As a first test of the apparent horizon finder, we use a single black hole in Kerr-Schild coordinates (see, e.g., [28]) to study its convergence properties and robustness. Let M and a denote respectively the mass and spin parameter of the black hole. In the standard spherical coordinates (r, θ, φ) , the polar and equatorial coordinate radii of the apparent horizon are given by

$$r_{\text{po}} = \bar{r}, \quad r_{\text{eq}} = \sqrt{\bar{r}^2 + a^2}, \quad (30)$$

where $\bar{r} = M + \sqrt{M^2 - a^2}$. The area is given by

$$A = 4\pi (\bar{r}^2 + a^2). \quad (31)$$

We first test the convergence property of the code with respect to increasing number of collocation points from runs with a black hole of $M = 1$ and $a = 0.9$. The polar radius of the apparent horizon is $r_{\text{po}} \approx 1.436$ and the equatorial radius is $r_{\text{eq}} \approx 1.695$. The analytic data $(\gamma_{\hat{i}\hat{j}}, K_{\hat{i}\hat{j}})$ are set on the numerical grid points of the computational domain ranging from $r = 1$ to $r = 5$, which is covered by three spectral domains. The boundary between the first and the second domains is at $r = r_{12} = 1.5$, whereas that between the second and the third domains is at $r = r_{23} = 2.5$. In each domain, we use $(N_r, N_\theta, N_\varphi)$ collocation points. We also enforce a symmetry with respect to the equatorial plane. The initial guess for h is a sphere at $r = 3$.

Table 1. Convergence test for a Kerr-Schild black hole with $M = 1$ and $a = 0.9$. Listed are the number of radial collocation points in each domain N_r , the fractional errors in the polar (equatorial) coordinate radius $\Delta r_{\text{po}}/r_{\text{po}}$ ($\Delta r_{\text{eq}}/r_{\text{eq}}$) and area $\Delta A/A$, the maximum remaining error of the expansion function $\Delta \Theta_{\text{max}}$ on the horizon and the run times. We use $N_\theta = (N_r + 1)/2$ points in the polar direction and $N_\varphi = 1$ in the azimuthal direction. We set the iteration parameter $\epsilon_h = 10^{-10}$.

N_r	$\Delta r_{\text{po}}/r_{\text{po}}$	$\Delta r_{\text{eq}}/r_{\text{eq}}$	$\Delta A/A$	$\Delta \Theta_{\text{max}}$	Time (s)
13	2.360×10^{-5}	8.003×10^{-6}	1.276×10^{-5}	4.240×10^{-3}	0.507
17	1.693×10^{-6}	9.705×10^{-8}	1.605×10^{-6}	5.333×10^{-4}	0.747
21	1.580×10^{-7}	2.145×10^{-8}	1.788×10^{-7}	6.574×10^{-5}	1.129
25	1.692×10^{-8}	4.235×10^{-9}	2.045×10^{-8}	8.033×10^{-6}	1.615
33	1.067×10^{-10}	1.707×10^{-10}	4.733×10^{-10}	1.559×10^{-7}	3.059
37	1.649×10^{-10}	1.325×10^{-10}	2.863×10^{-10}	2.383×10^{-8}	4.286
41	1.590×10^{-10}	1.053×10^{-10}	2.154×10^{-10}	3.790×10^{-9}	5.722

Table 1 shows the results for increasing N_r , with $N_\theta = (N_r + 1)/2$ and $N_\varphi = 1$. We choose the iteration parameter $\epsilon_h = 10^{-10}$ in this test (see section 4.2). In the table, for each N_r , we list the fractional errors in the polar (equatorial) coordinate radius $\Delta r_{\text{po}}/r_{\text{po}}$ ($\Delta r_{\text{eq}}/r_{\text{eq}}$) and area $\Delta A/A$, the maximum remaining error in the expansion function $\Delta \Theta_{\text{max}}$ on the horizon's surface, and the run times⁺. The error in the area is defined by $\Delta A/A := |(A_{\text{ana}} - A_{\text{num}})/A_{\text{ana}}|$, where the analytic result A_{ana} is given by equation (31) and the numerical result is calculated by the integral

$$A_{\text{num}} = \int_S \sqrt{\hat{q}} h^2 \sin \theta d\theta d\varphi, \quad (32)$$

with \hat{q} being the determinant of the 2-metric on the apparent-horizon's surface (expanded onto the basis $\{\mathbf{e}_i\}$). Explicitly, in terms of a general 3-metric γ_{ij} , A_{num} is given by

$$A_{\text{num}} = \int_0^{2\pi} \int_0^\pi [(\gamma_{\hat{r}\hat{r}} h_{,\theta}^2 + 2\gamma_{\hat{r}\hat{\theta}} h h_{,\theta} + \gamma_{\hat{\theta}\hat{\theta}} h^2) (\gamma_{\hat{r}\hat{r}} h_{,\varphi}^2 + 2\gamma_{\hat{r}\hat{\varphi}} h h_{,\varphi} \sin \theta + \gamma_{\hat{\varphi}\hat{\varphi}} h^2 \sin^2 \theta) - (\gamma_{\hat{r}\hat{r}} h_{,\theta} h_{,\varphi} + \gamma_{\hat{r}\hat{\theta}} h h_{,\varphi} + \gamma_{\hat{r}\hat{\varphi}} h h_{,\theta} \sin \theta + \gamma_{\hat{\theta}\hat{\varphi}} h^2 \sin \theta)^2]^{1/2} d\theta d\varphi. \quad (33)$$

In figure 1 we plot $\Delta A/A$ against N_r to explicitly show the convergence behaviour of the finder for three different choices of ϵ_h . It can be seen that the error $\Delta A/A$ converges exponentially towards zero with the number of points, as expected for spectral methods, until the accuracy is limited by the choice of ϵ_h . Furthermore, we also see that the number of iterations to a given error level ϵ_h is essentially independent of the value of ℓ_{max} used in equation (10). This agrees with the conclusions obtained from the original Nakamura *et al*'s algorithm (or its modifications) as investigated by Kemball and Bishop [23].

Next we test the robustness of our finder by performing runs with different initial guesses for h . We use the same black hole as above ($M = 1, a = 0.9$), but with a larger computational domain ranging from $r = 1$ to $r = 10$. The boundaries between the different spectral domains are $r_{12} = 2.5$ and $r_{23} = 5.5$. In general, we set up an

⁺ The run times correspond to the CPU time the code took to locate the apparent horizon on a 2 GHz Intel Core Duo processor. The best-fitted curve suggests that the scaling of the run time is close to N_θ^2 , which comes from the computation of discrete Legendre transforms.

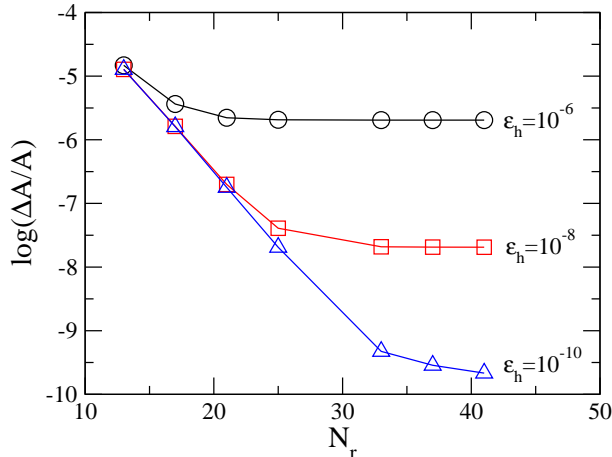


Figure 1. Convergence towards zero of the fractional error in the area $\Delta A/A$ with the number of collocation points for three different choices of the iteration parameter ϵ_h .

Table 2. Robustness test for the same black hole used in table 1. The polar coordinate radius of the apparent horizon is $r_{po} \approx 1.436$ and the equatorial coordinate radius is $r_{eq} \approx 1.695$. The initial guess for the 2-surface h is given by the surface of an ellipsoid with axes (a, b, c) defined in equation (34). We use collocation points $N_r = 25$ and $N_\theta = 13$ for all the five cases considered, but $N_\varphi = 1$ (4) for cases A and B (C-E).

Case	(a, b, c)	$\Delta A/A$ (10^{-6})
A	(8, 8, 8)	4.04871
B	(1.2, 1.2, 1.2)	4.04905
C	(4, 6, 8)	4.04875
D	(2, 3, 1.2)	4.04910
E	(1.2, 1.5, 2)	4.04909

initial guess for h to be the surface of an ellipsoid given by

$$\frac{x^2}{a^2} + \frac{y^2}{b^2} + \frac{z^2}{c^2} = 1, \quad (34)$$

where (x, y, z) are the Cartesian coordinates relating to the spherical coordinates (r, θ, φ) in the standard way. The constants (a, b, c) are freely chosen. The initial guess used for the results listed in table 1 corresponds to $a = b = c = 3$. Table 2 contains the results for five different initial guesses. Case A corresponds to a sphere with a coordinate radius which is about five times away from the horizon's surface. On the other hand, the initial surface for case B is a sphere located entirely inside the apparent horizon. The initial guess for case C is an ellipsoid enclosing the horizon. Finally, cases D and E represent initial surfaces which cross the horizon. The results show that our finder can locate the apparent horizon to the same accuracy with all the five (quite generic) choices of (a, b, c) .

One of the main requirements of an apparent horizon finder is speed. This is in particular an important issue if the finder has to run frequently during a simulation. In order to compare the speed of our finder with some other commonly used methods, we take the data given by Schnetter [18].

Table 3. Schwarzschild black hole offset from the coordinate origin. The hole is located at the Cartesian coordinates $(d/\sqrt{2}, d/\sqrt{2}, 0)$. Listed are the offset d , the fractional error in the area $\Delta A/A$, and the maximum remaining error of the expansion function on the horizon $\Delta\Theta_{\max}$.

d	$\Delta A/A$	$\Delta\Theta_{\max}$
0.1	9×10^{-6}	3×10^{-3}
0.2	3×10^{-6}	5×10^{-3}
0.3	2×10^{-6}	2×10^{-2}
0.4	1×10^{-4}	5×10^{-2}

In table 5 of [18] Schnetter compared the run times to locate the apparent horizon of a Kerr-Schild black hole with $M = 1$ and $a = 0.6$ for his elliptic method and two other methods, namely the fast-flow [22] and minimization [29] algorithms. The fastest case (0.5 s on a 1.2 GHz processor) was obtained by his elliptic method with the initial guess being a sphere at $r = 2$. The error in the area is $\Delta A/A = 9 \times 10^{-3}$ (according to table 4 of [18]). For comparison, the fast-flow and minimization algorithms took more than 10 s and 90 s respectively in the test [18].

We have performed tests with the same black hole and initial guess, and found that our finder took 0.129 s (on our 2 GHz processor) to locate the horizon to the accuracy $\Delta A/A = 2 \times 10^{-5}$ using the resolution $(N_r, N_\theta, N_\varphi) = (7, 5, 1)$ with $\epsilon_h = 10^{-8}$. We have also used Thornburg’s finder AHFINDERDIRECT [19] (which is implemented within the CACTUS computational toolkit [30]) to perform the same test using Cartesian grid resolutions $(N_x, N_y, N_z) = (31, 31, 19)$ with $\Delta x = \Delta y = \Delta z = 0.2$ in bitant symmetry. We found that his finder took 1.004 s (on our 2 GHz processor) to locate the apparent horizon to the accuracy $\Delta A/A = 3 \times 10^{-4}$.

We note that the above test does not represent a direct comparison between the different algorithms because of the different grid structures (Cartesian versus spherical coordinates), code implementations, memory usage and computer systems. Nevertheless, we can conclude that for this particular test, to obtain about the same accuracy level, our spectral-method-based finder is as efficient as the finders developed by Schnetter [18] and Thornburg [19].

5.2. Brill-Lindquist data

In this part, we test our finder using the Brill-Lindquist data [31]. This is a classic test involving multiple black holes used in numerical relativity. The 3-metric is conformally flat, $\gamma_{ij} = \phi^4 f_{ij}$, and is time symmetric (i.e. $K_{ij} = 0$). For two black holes, ϕ is given by

$$\phi = 1 + \frac{M_1}{2|\vec{r} - \vec{r}_1|} + \frac{M_2}{2|\vec{r} - \vec{r}_2|}, \quad (35)$$

where M_i ($i = 1, 2$) is the mass of the i th black hole and \vec{r}_i are the coordinate positions of the holes.

We first begin with a single black hole ($M_2 = 0$), in which case the problem is equivalent to a Schwarzschild black hole in isotropic coordinates offset from the coordinate origin. The apparent horizon is a coordinate sphere of radius $M_1/2$ with respect to the center of the hole. The area of the horizon is $A = 16\pi M_1^2$. We set $M_1 = 1$ and the coordinate position of the hole at $\vec{r}_1 = (x_1, y_1, z_1) = (d/\sqrt{2}, d/\sqrt{2}, 0)$. We have varied d in order to verify that our finder also works when the center of the spherical harmonics is offset from the center of the horizon. Table 3 lists the

results for four different values of d . The initial guesses are always $a = b = c = 1$ in equation (34). We use three spectral domains to cover the spatial slice up to $r = 1.5$, with collocation points $(N_r, N_\theta, N_\varphi) = (33, 17, 16)$ in each domain. The boundaries between the domains are $r_{12} = 0.5$ and $r_{23} = 0.8$. Similar to [22, 23], we see that the accuracy drops quite significantly for very distorted surfaces with respect to the coordinate origin. In particular, the error in the area $\Delta A/A$ increases by almost two orders of magnitude when d increases from 0.3 to 0.4; this error could be reduced using higher grid resolution*. Nevertheless, it is worth to point out that the original Nakamura *et al* spectral algorithm [17] would not produce any results for $d = 0.3$ and 0.4 because equation (15) has no roots [23]. We also see that the results are essentially independent of the direction of the offset.

Next we turn to Brill-Lindquist data for two black holes of equal mass. In particular, we take $M_1 = M_2 = 1$ in the test. The data forms a one-parameter family parameterized by the coordinate separation d between the holes. When they are far apart, each hole has an individual apparent horizon. For small separation, there is a single common apparent horizon enclosing both holes. Determining the critical separation at which the common horizon appears in this two black-hole spacetime is a standard test problem for apparent horizon finders. The critical separation obtained originally by Brill and Lindquist is $d_c = 1.56$ [31], while more recent results suggest that $d_c \approx 1.53$ (e.g., [19, 23, 32, 33]). In particular, we note that Thornburg [19] and Shoemaker *et al* [33] report very close results at $d_c = 1.532$ and $d_c = 1.535$ respectively. Nevertheless, Thornburg reports $A = 196.407$ for the area of the critical apparent horizon, which is quite different from the value $A = 184.16$ obtained by Shoemaker *et al*.

Here we test our finder by trying to find a common horizon at the critical separations, as reported by Thornburg [19] and Shoemaker *et al*. [33]. The black holes are on the z -axis, with their centers at $z = \pm d/2$. In the test, we use four spectral domains to cover the spatial slice up to $r = 2$. The boundaries between the domains are $r_{12} = 0.5$, $r_{23} = 1$ and $r_{34} = 1.5$. The initial guesses are $a = b = c = 2$ in equation (34). We use $(N_r, N_\theta, N_\varphi) = (41, 31, 1)$ in each domain and the iteration parameter $\epsilon_h = 10^{-6}$. Our finder reports a common horizon at $d = 1.532$ (Thornburg's critical value) with the area of that horizon determined to be $A = 196.417$, which agrees to Thornburg's value to 0.005%. The maximum remaining error of the expansion function on the horizon is $\Delta\Theta_{\max} = 7 \times 10^{-4}$. The finder took 59.2 s to locate the horizon. We note that increasing ϵ_h to 10^{-4} would reduce the run time to 23.3 s, without changing the three significant figures of A . On the other hand, for the same grid setting and parameters, our finder does not find a common horizon at the critical value $d = 1.535$ reported by Shoemaker *et al*. In general, for $d > 1.532$, we find two disjoint apparent horizons surrounding \vec{r}_1 and \vec{r}_2 by setting the coordinate origin for the apparent horizon finder (see section 2) separately at around the points \vec{r}_1 and \vec{r}_2 . In figure 2 we show the position of the common apparent horizon on the x - z plane for the case $d = 1.532$. The results obtained by four different values of N_θ (with $N_r = 41$ and $N_\varphi = 1$ fixed) are plotted together to show the convergence of the horizon.

* The error $\Delta A/A$ drops down to 2×10^{-5} for the case $d = 0.4$ using collocation points $(N_r, N_\theta, N_\varphi) = (33, 25, 24)$.

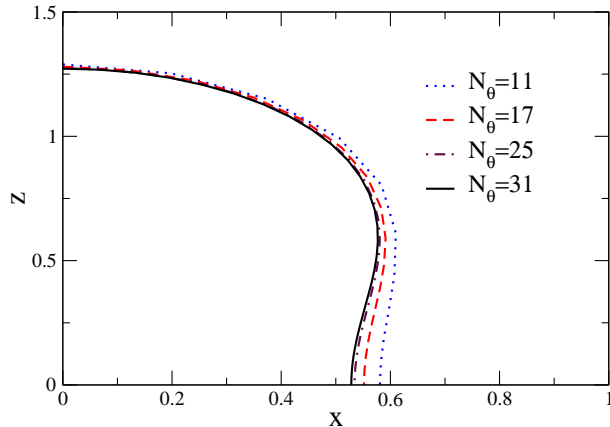


Figure 2. Position of the common apparent horizon on the x - z plane for Brill-Lindquist data with $d = 1.532$. The black holes are centered at $z = \pm d/2$ along the z -axis. The results obtained by four different values of N_θ are shown (with $N_r = 41$ and $N_\varphi = 1$ fixed).

6. Conclusions

In this paper we have presented a new apparent horizon finder which is based on spectral methods. Our proposed algorithm does not need to treat the $\ell = 0$ coefficient of the spherical harmonics decomposition separately as required in previous spectral apparent horizon finders [17, 23]. Hence, this leads to a faster and more robust finder based solely on spectral methods. We have made a performance comparisons with other apparent horizon finders using the Kerr-Schild data. Our finder is much faster (by orders of magnitude) than other commonly used methods (e.g., the fast-flow and minimization algorithms). It is also as efficient as the currently fastest methods developed recently by Schnetter [18] and Thornburg [19]. We have also shown that our finder is capable of locating the horizon of a shifted Schwarzschild black hole with a large offset from the coordinate origin. This would not be possible by using the original Nakamura *et al* spectral algorithm [17] because equation (15) has no roots if the offset is too large. We have also tested our finder for a two black-hole spacetime using the Brill-Lindquist data. In particular, we have verified previous results on the critical separation at which a common horizon appears in this spacetime.

Our apparent horizon finder is implemented within the C++ library LORENE for numerical relativity [27], and is freely available. The finder should be easily adopted in spectral-method-based evolution codes [24, 34, 35, 36], particularly to those using shell-like domains in spherical coordinates. Comparing to other freely available apparent horizon finders which are based on the finite-differencing method (AHFINDER [32] and AHFINDERDIRECT [19]), our finder also represents another option available to finite-differencing evolution codes, with some interpolation to be implemented between the finite-difference and spectral grids as, for example, in [37].

Note added: After we have submitted the paper, Tsokaros and Uryū informed us that they had recently developed an apparent horizon finder based on the same formulation presented in this paper [38]. Their work and ours were done independently.

Acknowledgments

We thank José Luis Jaramillo for very helpful discussions. We also thank Antonios Tsokaros and Kōji Uryū for bringing their work [38] to our attention. LML is supported in part by the Hong Kong Research Grants Council (Grant No: 401905 and 401807) and a postdoctoral fellow scheme at the Chinese University of Hong Kong. JN was supported by the A.N.R. grant 06-2-134423 entitled “Mathematical methods in general relativity” (MATH-GR).

References

- [1] Hughes S A, Keeton C R, Walker P, Walsh K T, Shapiro S L, and Teukolsky S A 1994 *Phys. Rev. D* **49** 4004
- [2] Anninos P, Bernstein D, Brandt S, Libson J, Massó J, Seidel E, Smarr L, Suen W-M, and Walker P 1995 *Phys. Rev. Lett.* **74** 630
- [3] Libson J, Massó J, Seidel E, Suen W-M, and Walker P 1996 *Phys. Rev. D* **53** 4335
- [4] Diener P 2003 *Class. Quantum Grav.* **20** 4901
- [5] Hawking S W and Ellis G F R 1973 *The Large Scale Structure of Space-Time* (Cambridge: Cambridge University Press)
- [6] Unruh W G 1984 as cited in [7]
- [7] Thornburg J 1987 *Class. Quantum Grav.* **4** 1119
- [8] Seidel E and Suen W-M 1992 *Phys. Rev. Lett.* **69** 1845
- [9] Alcubierre M, Brügmann B, Diener P, Koppitz M, Pollney D, Seidel E, and Takahashi R 2003 *Phys. Rev. D* **67** 084023
- [10] Campanelli M, Lousto C O, Marronetti P, and Zlochower Y 2006 *Phys. Rev. Lett.* **96** 111101
- [11] van Meter J R, Baker J G, Koppitz M, and Choi D-I 2006 *Phys. Rev. D* **73** 124011
- [12] Baiotti L and Rezzolla L 2006 *Phys. Rev. Lett.* **97** 141101
- [13] Ashtekar A and Krishnan B 2004 *Living Rev. Relativity* **7** 10
- [14] Booth I 2005 *Can. J. Phys.* **83** 1073
- [15] Gourgoulhon E and Jaramillo J L 2006 *Phys. Rev. D* **74** 087502
- [16] Thornburg J 2005 *Preprint* gr-qc/0512169
- [17] Nakamura T, Kojima Y, and Oohara K 1984 *Phys. Lett.* **106A** 235
- [18] Schnetter E 2003 *Class. Quantum Grav.* **20** 4719
- [19] Thornburg J 2004 *Class. Quantum Grav.* **21** 743
- [20] Baumgarte T W and Shapiro S L 2003 *Phys. Rep.* **376** 41
- [21] Bonazzola S, Gourgoulhon E, and Marck J-A 1998 *Phys. Rev. D* **58** 104020
- [22] Gundlach C 1998 *Phys. Rev. D* **57** 863
- [23] Kembal A J and Bishop N T 1991 *Class. Quantum Grav.* **8** 1361
- [24] Bonazzola S, Gourgoulhon E, Grandclément P, and Novak J 2004 *Phys. Rev. D* **70** 104007
- [25] Shibata M 1997 *Phys. Rev. D* **55** 2002
- [26] Bonazzola S, Gourgoulhon E, and Marck J-A 1999 *J. Comput. Appl. Math.* **109** 433
- [27] <http://www.lorene.obspm.fr/>
- [28] Misner C W, Thorne K S, and Wheeler J A 1973 *Gravitation* (San Francisco: Freeman)
- [29] Anninos P, Camarda K, Libson J, Massó J, Seidel E, and Suen W-M 1998 *Phys. Rev. D* **58** 024003
- [30] <http://www.cactuscode.org>
- [31] Brill D R and Lindquist R W 1963 *Phys. Rev.* **131** 471
- [32] Alcubierre M, Brandt S, Brügmann B, Gundlach C, Massó J, Seidel E, and Walker P 2000 *Class. Quantum Grav.* **17** 2159
- [33] Shoemaker D M, Huq M F, and Matzner R A 2000 *Phys. Rev. D* **62** 124005
- [34] Scheel M A, Erickcek A L, Burko L M, Kidder L E, Pfeiffer H P, and Teukolsky S A 2004 *Phys. Rev. D* **69** 104006
- [35] Tichy W 2006 *Phys. Rev. D* **74** 084005
- [36] Boyle M, Lindblom L, Pfeiffer H P, Scheel M A, and Kidder L E 2007 *Phys. Rev. D* **75** 024006
- [37] Dimmelmeier H, Novak J, Font J A, Ibáñez J M, and Müller E 2005 *Phys. Rev. D* **71** 064023
- [38] Tsokaros A A and Uryū K 2007 *Phys. Rev. D* **75** 044026